

The displacement of bridge abutments on clay

M.D. Bolton & H.W. Sun

Engineering Department, Cambridge University, UK

ABSTRACT: The behaviour of spread base abutments on firm to stiff clay have been investigated by centrifuge model experiments, which involve embankment building and bridge deck loading simulation. Wall movements during undrained foundation response and consolidation under the new embankment were observed and back-analysed. Stiffness response of the one-dimensionally consolidated clay is deduced from plane strain element tests and stress history analyses. Stress path direction and stress-strain history is found to be important for the calculations of undrained ground deformations based on a plastic deformation mechanism, and subsequently in the estimation of wall displacement. Long-term wall movements are shown to be influenced by the rigidity of the wall and the granular backfill, so that inevitable differential settlement of the wall base leads to backward rotation and forward sliding at the base while the wall crest is inhibited from moving into the backfill. This causes increase of bending moment in the stem, but the limit of the horizontal thrust on the stem can be estimated from the sliding resistance of the base.

1 INTRODUCTION

Designers frequently want advice on problems of soil-structure interaction, which may involve the prediction of small but significant ground movements subject to complex load cycles. This paper describes an investigation of one such problem which demonstrates that centrifuge models can be used to clarify behaviour and suggest analytical approaches. Bridge abutments with spread foundations over clay, figure 1, have been found to be acceptable if the clay is stiff enough, leading to considerable economies through the avoidance of piles. Many designers are unwilling to risk the possibility of unserviceability through lateral displacement of the abutment, however, especially since calculation procedures for horizontal movements are not well established (FHWA 1985). Centrifuge tests on the balanced beam centrifuge at the Cambridge University Geotechnical Centrifuge Centre were sponsored by the UK Transport and Road Research Laboratory for the investigation of model abutments on clay.

2 CENTRIFUGE TESTS

Centrifuge modelling is useful in identifying soil-structure interaction at reduced scale and providing data on an idealized prototype for the development of analytical techniques. In the investigation of the interaction of a spread base abutment wall and its embankment fill on a clay foundation, five centrifuge model tests were performed on the Cam-

bridge University 10m beam centrifuge (Schofield 1980). Figure 2 shows a typical 1/100 centrifuge model from this series of experiments on firm to stiff kaolin clay. The clay was initially consolidated to a maximum vertical pressure of 660kPa in a consolidometer, and then allowed to swell back to a vertical pressure of 66kPa before the clay was removed from the consolidometer and trimmed to the dimensions of the model. The clay model was then placed in the strongbox, and the front surface was marked with a matrix of black plastic bullets, which were used to measure subsoil displacements from photographs taken through the Perspex window in-flight.

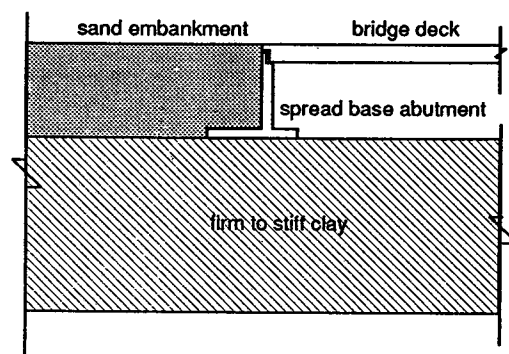


Figure 1 Spread base abutment wall on clay

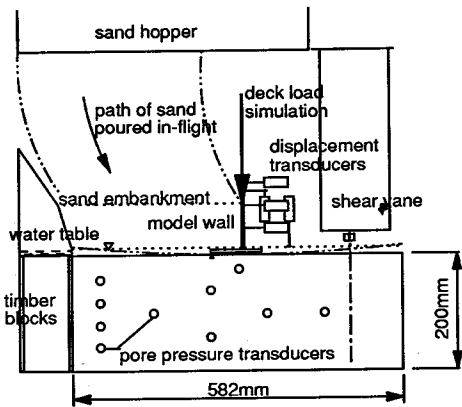


Figure 2 A typical centrifuge model

Figure 3 shows the configuration of the aluminium model walls used in the tests. The 5.5mm thick model wall is designed to simulate the long-term bending stiffness of a 1m thick reinforced concrete section, and the 8mm thick section of wall L2 simulates the short term bending stiffness of the same prototype. The model wall was instrumented with 13 bending moment transducers. Seven displacement transducers were used to monitor the displacement of the wall and one to measure ground settlement in front of the wall base. These measurements are projected in terms of vertical and horizontal displacement, and rotation, of a reference point, figure 4.

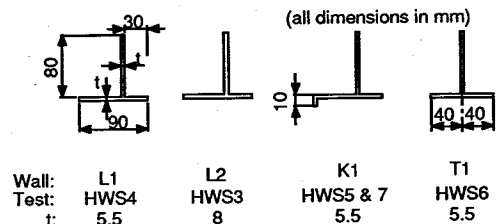


Figure 3 Model abutment walls

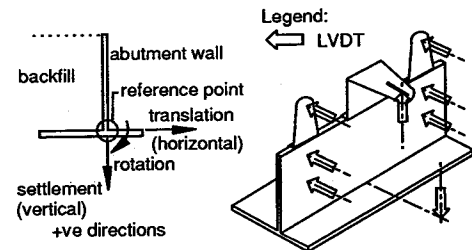


Figure 4 Wall movement measurement

After the clay foundation reached pore pressure equilibrium by continuous swelling near the top and re-compression near the bottom, figure 5, shear vane tests were conducted at different depths in the clay foundation to measure the consistency of the model. Figure 6 shows the undrained shear strength profile measured by in-flight shear vane tests.

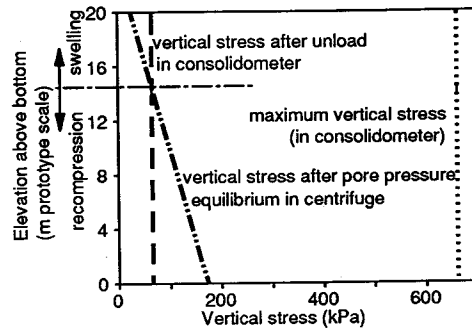


Figure 5 Vertical stress state of clay foundation

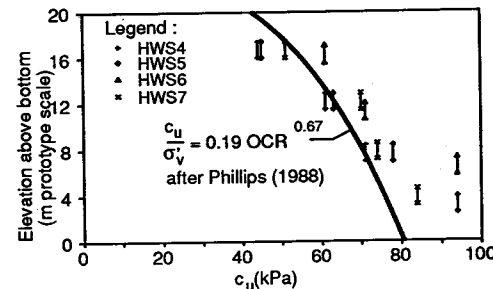


Figure 6 Undrained Shear Strength Profile of clay foundation

Then, a sand embankment was placed in-flight by pouring sand from a hopper located above the model. Embankment construction caused an immediate heave, forward translation and backward rotation of the wall reference point. Forward translation of the wall causes the lateral pressure to drop to the active value mobilizing its critical shear strength. Figure 7 plots bending moments in the wall stem measured in tests HWS3 to HWS7 and the prediction by a linear pressure distribution with $k_a=0.271$ ($\phi=35^\circ$).

Figure 8 shows the displacements of the clay foundation just after the embankment construction was completed in test HWS3, revealed by measuring the in-flight photographs before and after sand-pouring.

Consolidation of the model clay foundation took place in the next 5.5 to 6 hours (6 years and 3 months to 6 years and 10 months at prototype scale). Ground displacement due to consolidation was mainly one-dimensional settlement as observed from

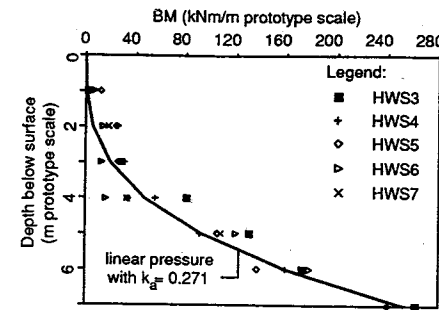


Figure 7 Bending moment on wall stem immediately after embankment building

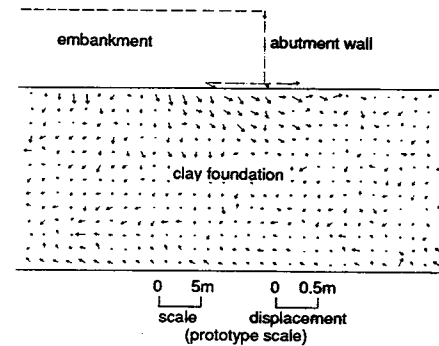


Figure 8 Subsoil displacement immediately after embankment construction in test HWS3

the in-flight photographs. Figure 9 shows the incremental subsoil displacement between undrained and consolidated states in test HWS3. At this stage, the abutment base rotated backwards to follow the ground settlement profile. Backward movement into the stiff backfill was prevented at the top of the wall which caused the wall base to move further outwards. A significant increase of bending moment in the wall stem was observed, figure 10 shows a part of the bending moment time record of test HWS7.

Vertical bridge deck loading on the wall stem was simulated after embankment construction in tests HWS5 to HWS7. It was achieved by the application of cycles of quasi-static live load superimposed on a "dead-load" base line by two pneumatic jacks located above the wall stem, figure 11. It was found in the test that the first application of the "dead-load" and the first cycle of the heavy live load each caused a slight change in wall movement and bending moment on the stem. These effects remained after the removal of the live load but the influences of subsequent cycles of live load were insignificant, except the instantaneous response from the bending moment transducers on the wall base. This can be explained by the high stiffness on unloading and reloading in the clay foundation and backfill. Sun (1990) describes the centrifuge tests in more detail.

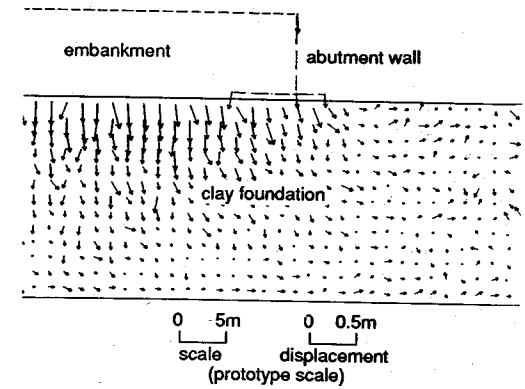


Figure 9 Subsoil displacement due to consolidation under embankment load in test HWS3

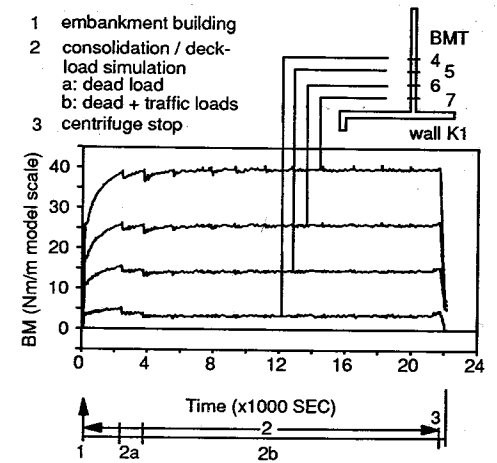


Figure 10 Bending moment time record of test HWS7

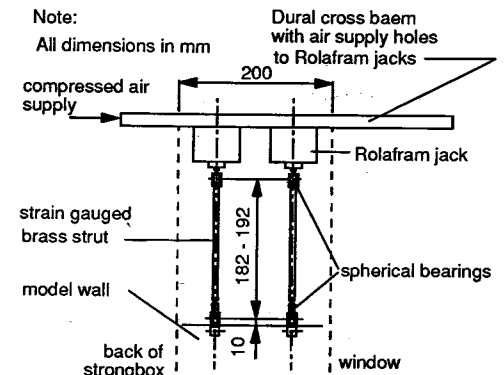


Figure 11 Deck-load simulator

3 STIFFNESS RESPONSE OF THE CLAY

The stress-strain response of an over-consolidated clay, which remains within the yield surface defined by its maximum consolidation pressure, is not linearly elastic. Non-linearity and anisotropy of the soil depend on the inherent anisotropy of its particle structure and the induced anisotropy of its current stress-path direction, stress and strain history.

Active and passive undrained cyclic stress path tests on vertical and horizontal plane-strain samples, as described in Sun (1990), show different stress-strain responses which reflects the strong inherent anisotropy in stiffness of the one-dimensionally consolidated kaolin, figure 12, where the change of mobilized shear strength Δc is defined in figure 13. Cyclic stress-strain response following an imposed reversal of loading is less affected by unknown stress-strain history during the sampling and setting-up processes. It is then necessary to select an origin for strain depending on whether the construction process reverses the prior strain direction in the model, or not.

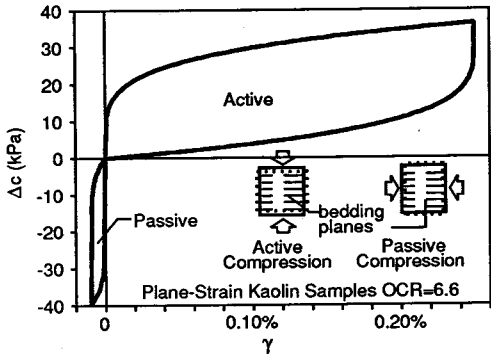


Figure 12 Undrained cyclic stress-strain response of over-consolidated kaolin

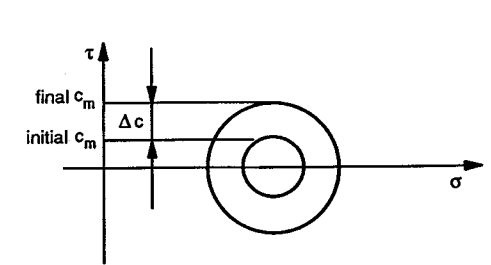


Figure 13 Mobilized shear strength of soil

Based on a stress and strain history analysis of the one-dimensional swelling and re-compression of the clay model, figure 14, the magnitude and sign of volumetric strain in the clay model since the last strain reversal can be estimated based on Al-Tabba (1988). In one-dimensional deformation, volumetric

strain is equal to shear strain, figure 15(a). Despite the difference in strain path direction, this shear strain is taken to be equivalent to undrained shear strain in this analysis, figure 15(b). Figure 16 shows the pre-strain profile in the clay model based on one-dimensional deformation from the last strain reversal. This pre-strain must be added to the newly imposed strain if that strain continues in the same direction. If the strain in the model reverses, the cyclic data of figure 12 can be applied directly without shifting the strain origin. Figure 17 shows the expected undrained stress-strain response of the model clay elements at different depths. The potential significance of high stiffness after strain reversal is clear. Note also in figure 17 that the element representing 4m depth, which had most recently been swelling, shows high stiffness in active loading, while that from the element representing 8m depth, which had most recently been consolidating, shows the opposite.

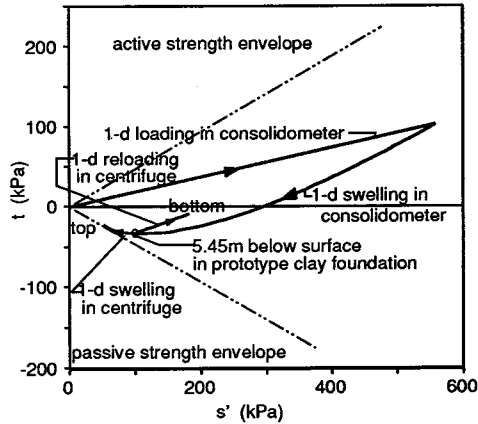


Figure 14 Stress history of centrifuge clay model

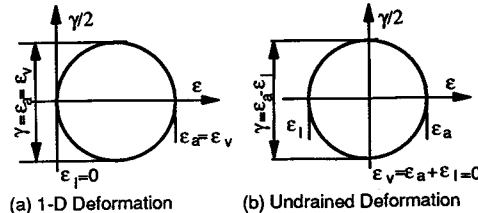


Figure 15 Mohr's circles of strain

In the simplest case, an idealized regional deformation mechanism consists of an active and a passive region, with a frictionless wound in-between, figure 18 (Bolton et al 1989). Vertical compression response from an active stress path is different from that of horizontal compression response from a passive stress path, figure 19. Displacement compatibility causes the same amount of shear strain in

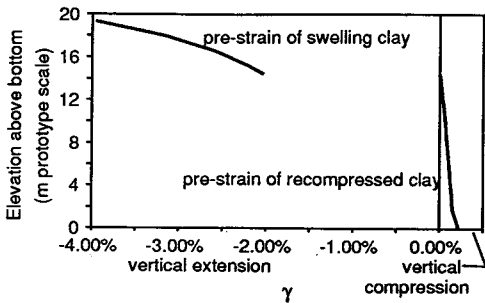


Figure 16 Pre-strain in clay foundation prior to embankment construction

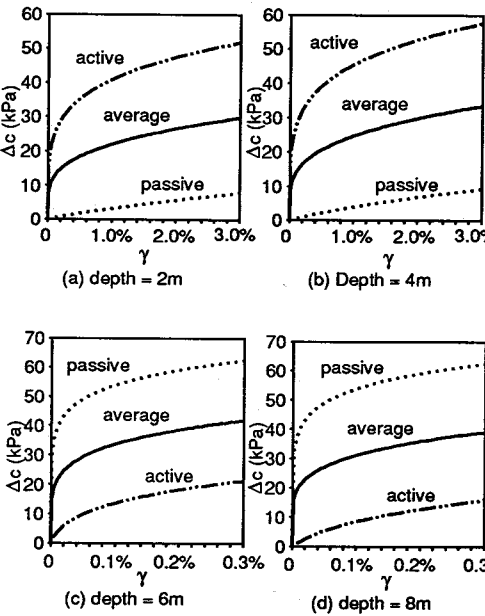


Figure 17 Stress-strain responses of clay elements

both zones. At the same shear strain, the active zone mobilizes additional shear stress Δc_1 , and the passive zone mobilizes Δc_2 , figure 19. Equilibrium and displacement compatibility are both approximately satisfied if an average stress-strain response is used for both active and passive zones with $\Delta c = 1/2(\Delta c_1 + \Delta c_2)$.

Predominant anisotropy in vertical strain was also observed in the consolidation phase of clay specimens which had been subjected undrained to either vertical or horizontal major stress changes in the plane strain element tests. This helped to explain the dominance of vertical displacement in the consolidation of the clay foundation, figure 9.

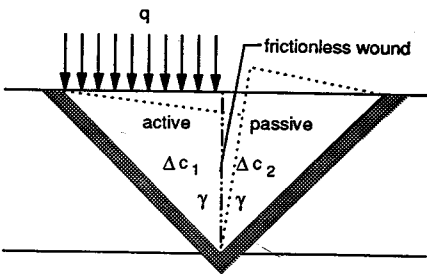


Figure 18 A simple deformation mechanism for undrained surcharge

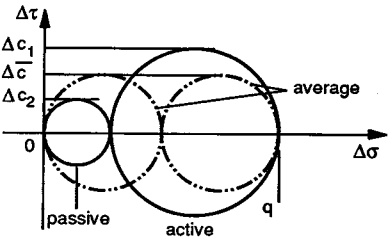


Figure 19 Stress increments in the simple deformation mechanism

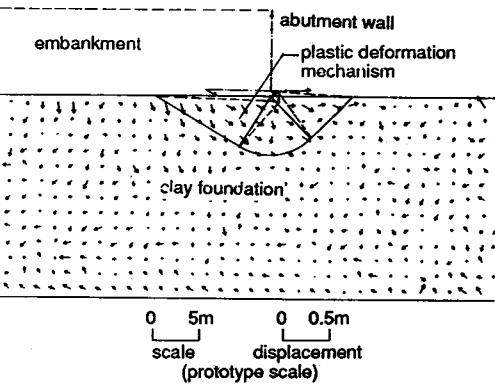


Figure 20 Undrained subsoil displacement and its prediction - test HWS3

4 GEO-STRUCTURAL MECHANISMS

An elementary extension to the conventional plasticity bearing capacity calculation has led to the development of a plastic deformation mechanism calculation for the estimation of undrained soil displacement under the embankment. Figure 20 shows the ground movement immediately after the embankment was built, revealed by spot-chasing from the in-flight photograph in test HWS3. The configuration of the plastic mechanism in undrained ground deformation is superimposed on the figure.

In order to simplify the calculations, an average additional shear strength $\Delta\bar{c}$ is assumed to be mobilized everywhere in the mechanism. The average stress-strain response at 2.7m depth below ground surface derived from both active and passive stress path responses within the mechanism, figure 21, is adopted in the analyses. This only causes a small equilibrium error, depending on the size of the active zone compared with the size of the whole mechanism, which is ignored in this case.

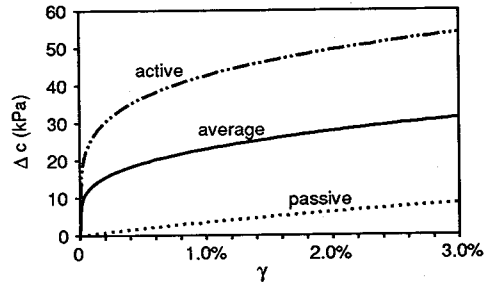


Figure 21 Stress-strain response of clay element at 2.7m below ground surface

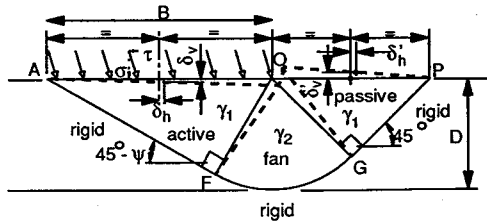


Figure 22 Plastic deformation mechanism for embankment on clay

The transition between swelling and recompression of the centrifuge clay model at 5.4m (prototype scale) below the ground surface causes a sharp ($\times 10$) increase of average of the active and passive stiffness of the clay below this point. Therefore, the depth D of the mechanism will not be expected to exceed 5.4m (prototype scale). The width B of the active block and depth D of the mechanism, figure 22, can be related by:

$$D = \frac{B}{\sqrt{2}} (\cos \Psi - \sin \Psi) \quad (1)$$

where $\Psi = 0.5 \sin^{-1} \left(\frac{\tau}{\Delta c} \right)$

The ground surface movement is linked to shear strain increment γ in the active and passive zones. The ground surface movement δ_v and δ_h at the middle of width B is given by:

$$\delta_v = 0.25 \gamma B (\cos \Psi - \sin \Psi)^2 \quad (2)$$

$$\delta_h = 0.25 \gamma B (\cos^2 \Psi - \sin^2 \Psi) \quad (3)$$

and the movement δ'_v and δ'_h at the middle of the passive zone ground surface is given by:

$$\frac{-\delta_v}{\delta'_v} = \frac{\delta_v}{\delta'_h} = \cos \Psi + \sin \Psi \quad (4)$$

The equilibrium equation links the surface loading to the average additional shear strength $\Delta\bar{c}_m$ mobilized within the zone of deformation:

$$\sigma = \Delta\bar{c} + \Delta\bar{c} \left(\pi - \sin^{-1} \frac{\tau}{\Delta\bar{c}} \right) + \sqrt{\Delta\bar{c}^2 - \tau^2} \quad (5)$$

The relationship between the ratio of shear and normal stress and the angle Ψ in figure 22 is given by equation 6 and is charted on figure 23.

$$\frac{\tau}{\sigma} = \frac{\sin 2\Psi}{1 + \pi - 2\Psi + \cos 2\Psi} \quad (6)$$

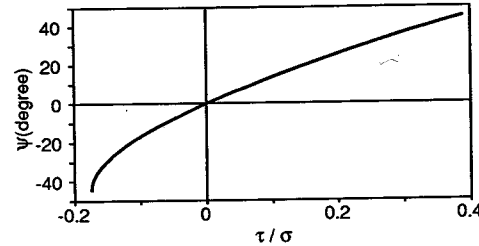


Figure 23 Effects of shear stress ratio on Ψ from equation (6)

Figure 24 represents the condition in test HWS7: wall K1 sitting on the clay foundation and retaining the edge of the newly constructed embankment. There is increasing outward horizontal displacement toward the edge of the embankment along the width B of the deformation mechanism. As only a very small shear strain is required to cause the backfill to adopt an active state, the lateral earth pressure acting in the backfill above the extending width B of the mechanism can be regarded as active for the equilibrium calculation. Although there should be no change of lateral pressure in the backfill above the zone from the heel of the wall to the farthest reach of the deformation mechanism, this length is relatively short in this particular case. Then, the horizontal traction τ is assumed to be distributed evenly on the width B of the deformation mechanism, in order to balance the lateral pressure in the backfill. For test HWS7, vertical surcharge on the width B is equal to $\sigma = 100 \times 16.4 \text{ kN/m}^3 \times 0.073 \text{ m} = 120 \text{ kN/m}^2$, and the horizontal traction $\tau = 0.5 \times k \times \sigma \times 100 \times 0.073 \text{ m} / B = 118.7 / B \text{ kN/m}^2$ where $k=0.271$. Solving equations 1 and 6 together with σ and τ , angle Ψ is found to be 13.12° and B is 10.22m. $\Delta\bar{c}$ is found to be 26.2 kN/m^2 from equation 5, then shear strain $\gamma = 1.6\%$ can be read from the stress-strain

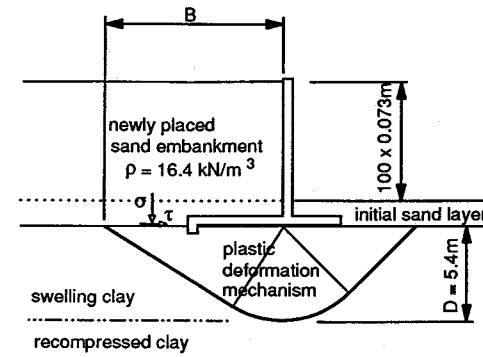


Figure 24 Undrained ground deformation mechanism for wall movement prediction

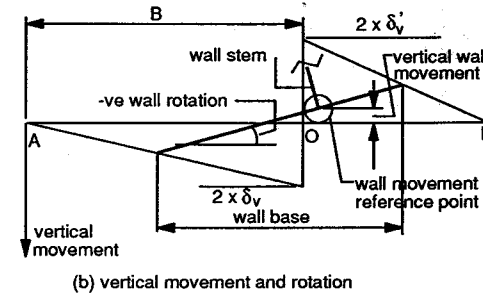
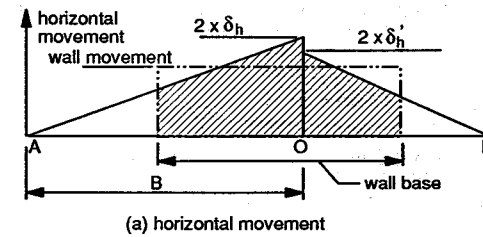


Figure 25 The estimation of wall movement from ground deformation under the base

diagram, figure 21. Finally, $\delta_v = 0.023 \text{ m}$, $\delta_h = 0.037 \text{ m}$, $\delta'_v = 0.031 \text{ m}$ and $\delta'_h = 0.031 \text{ m}$ is calculated from equations 2 to 4.

To convert ground movements underneath the wall base into prediction of wall movement, some simplifications were made. Horizontal movement of the wall was assumed to be the average value of the ground surface movement under the base, figure 25(a), and no relative slippage between subsoil and wall base was expected. Rotation of the wall was calculated from the vertical ground movements of the points on the soil surface at the edges of the wall base, figure 25(b). Vertical movement of the wall was estimated from the wall rotation and ground movement at the edges of the wall base, figure

25(b). Figure 26 compares the prediction and the test results. Wall movements during undrained foundation response caused by the embankment construction in other tests in this series of centrifuge experiments are also analysed similarly and their comparisons with the test results are summarized in Table 1.

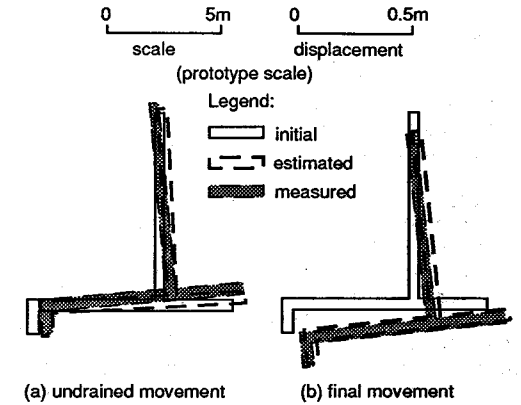


Figure 26 Wall movements in test HWS7

Table 1 Predicted and actual undrained wall movements in tests HWS3 to HWS7

Test No		HWS3	HWS4	HWS5	HWS6	HWS7
Wall		L2	L1	K1	T1	K1
Prediction	Horizontal (m)	0.042	0.042	0.045	0.051	0.051
	Vertical (m)	-0.012	-0.014	-0.015	-0.000	-0.015
	Rotation	-0.56%	-0.57%	-0.59%	-0.70%	-0.60%
Experimental	Horizontal (m)	0.066	0.053	0.047	0.044	0.047
	Vertical (m)	-0.044	-0.012	-0.036	-0.033	-0.040
	Rotation	-1.03%	-0.93%	-0.74%	-0.44%	-0.85%

Although the pattern of subsoil movement was closely followed by the plastic ground movement prediction model, the predictions of wall movements may not seem very accurate in terms of percentage errors (36% maximum error in horizontal movement, 100% maximum error in vertical movement and 59% maximum error in wall rotation) or in absolute terms of prototype scale. However, these movements are very small at model scale, about 0.5mm maximum. Small differences may contribute to large percentage or prototype scale errors. Of course, the discrepancy may also be due to the assumptions made in the simplified procedure to convert ground movements to wall movement. The actual deformation pattern in the sub-soil may have been modified by the presence of the wall base, and the effects of excess pore water pressure distribution in the model tests can cause some changes in foundation soil deformation. The ability of this simple calculation procedure in predicting the cor-

rect order of magnitude of ground and wall movements nevertheless makes it a useful tool for routine serviceability design calculations.

Pore pressure changes measured in the over-consolidated clay beneath the newly constructed embankment were found to match the prediction of elastic solution rather closely. This corresponds with the observations of negligible pore pressure changes during the active cyclic shear tests reported in figure 12. Apparently, the plastic shear behaviour does not involve the tendency for volumetric change for these stress cycles. One dimensional settlement calculations based on the dissipation of the estimated pore pressure were found to agree with test results. Differential settlement at the edge of the embankment caused the wall to rotate backwards forcing the stem to press into the backfill. As the foundation clay is less stiff than the backfill in this mode of movement, the top of the wall stem remained on the same vertical plane while the base moved out. Figure 26 shows the predicted final wall movement against the test result in test HWS7, based on the settlement profile estimation and the displacement compatibility of the wall, its clay foundation and the stiff backfill. Also, the relative displacement between the backfill and the wall, which was caused by its backward rotation, induced an increase of the lateral earth pressure acting behind as shown by a significant increase of the bending moments in the wall stem. A limit on the total lateral thrust on the wall stem is given by the base sliding resistance. Table 2 shows the estimated limits of lateral pressure on the wall stem compared with the test results. The limiting k values in tests HWS5 and HWS7 are much higher than their test results. A shear key, present in these tests, was responsible for the higher estimate of sliding resistance. However, the wall movement in these tests could have been controlled by regional soil deformation, rather than by local sliding under the wall base.

Table 2 Predicted limits and measured final lateral earth pressure on wall stems in tests HWS3 to HWS7

Test No	HWS3	HWS4	HWS5	HWS6	HWS7
Wall	L2	L1	K1	T1	K1
k_{limit} (predicted)	0.59	0.60	0.64	0.53	0.73
k_{final} (measured)	0.58	0.50	0.40	0.45	0.45

5 CONCLUSIONS

In-flight probes, such as vanes or penetrometers, are essential for proving the consistency and strength of model soil deposits. If the objective of model tests is to clarify deformation modes, or serviceability criteria, however, strength data must be supplemented by appropriate strain path tests on soil elements. Stiffness errors of a factor of 10 could otherwise be almost inevitable.

Real soil deformation in centrifuge models or in

the field are often more localized than those predicted by elementary elastic finite element computations. Plastic deformation mechanisms based on the method of characteristics resembled patterns of undrained deformation in the models. Furthermore, the magnitude of undrained soil displacements have been predicted by deducing mobilized soil strengths, and relating these to shear strain increments observed in stress-path tests. The accuracy of this modified plastic approach to displacement prediction of abutment walls is apparently sufficient to form the basis of a design method.

The model walls displayed negligible displacement at the elevation of the bridge deck in the later phase of backward rotation due to consolidation beneath the new embankment. This was attributed to the relative stiffness of the backfill, in comparison with the clay foundation. Although this observation relieves anxiety regarding the bridge bearings, it brings an additional bending moment in the wall stem, which can be accounted for.

ACKNOWLEDGEMENTS

The work described here was supported by a research contract let by the Transport and Road Research Laboratory of the UK Department of Transport. The opinions expressed here are the authors' and do not necessarily coincide with those of the Laboratory or the Department.

Wing Sun is grateful for the financial support of the Croucher Foundation of Hong Kong, and the Overseas Research Student Award from the CVCP of British Universities.

REFERENCES

- Al-Tabbaa, A. 1988. Permeability and Stress-Strain Response of Speswhite Kaolin, PhD Dissertation, Cambridge University, UK.
- Bolton, M.D., Springman, S.M. and Sun, H.W. 1990. The Behaviour of Bridge Abutments on Clay, Proceedings of Design and Performance of Earth Retaining Structures, ASCE Geotechnical Special Publication No 25.
- Phillips, R. 1988. Centrifuge Lateral Pile Tests in Clay, Tasks 2 & 3, a Report to Exxon Production Research Corp. by Lynxvale Ltd., Cambridge, UK.
- Schofield, A.N. 1980. Cambridge University Geotechnical Centrifuge Operations, *Geotechnique*, 30 (3), 1980, 227-268.
- Sun, H.W. 1990. Ground Deformation Mechanisms for Soil-Structure Interaction, PhD Dissertation, Cambridge University, UK.
- U.S. Department of Transportation, 1985. Tolerable Movement Criteria for Highway Bridges. Final Report FHWA/RD-85/107, Federal Highway Administration, USA.